Chapter 3

Concept and Numerical Simulations of Multi-Beam Linear Accelerators EVT with Depressed Collector for Drive Beam

Vladimir E. Teryaev

Additional information is available at the end of the chapter

http://dx.doi.org/10.5772/intechopen.70956

Abstract

The concept of the electron multi-beam linear accelerator electron voltage transformer (EVT) invokes aspects of a two-beam accelerator. Here, effective transformation of energy of several drive beams to energy of a high voltage accelerated beam takes place. It combines an RF generator and essentially an accelerator within the same vacuum envelope. Acceleration occurs in inductively-tuned cavities. The ratios between values of RF beam currents and their voltages are similar to ratios for an electric transformer that is leaded to dub this device an electron voltage transformer (EVT). Properties and high efficiency of the EVT accelerator proves to be true by the example of numerical simulations of three accelerator configurations generating electron beams with energies 1, 2 and 4.3 MeV, respectively. The submitted results of numerical simulations show a resource for the further increase in efficiency of the EVT accelerator up to 70–75% by using a depressed collector for a spent dive beam.

Keywords: two-beam accelerator, electron gun, drive beam, accelerated beam, RF buncher, accelerating cavity, depressed collector

1. Introduction

Two-beam linear collider can serve as the most known example use of two-beam concept in the field of high energy physics [1]. Derbenev Ya et al. [2] can serve as an example of consideration of the two-beam concept in the range of low energy (1–10 MeV). Specificity of low energy when the relativistic factor is low is that a change of velocity of particles for conservation of the appropriate phase ratio between drive bunches and accelerated bunches, i.e. for keeping of synchronism in process of beam-beam interactions, shall be taken into account. Derbenev Ya et al. assumed that the use of the H_{020} mode in a pill-box cavity where acceleration occurs on

an axis of the cavity and the annular drive beam changes its radius during movement [2]. Synchronization is carried out due to change in a focusing magnetic field along the axis of the device and this implies changing of the radius of the annular drive beam. However, this concept has never been developed any further.

Here, a new concept of the electron accelerator briefly named electron voltage transformer (EVT) is considered, where the multi-beam approach is of a crucial importance. The approach to use several beam-lets interacting with the common cavity is well-known and is implemented successfully in multi-beam klystrons (MBK's) [3, 4]. Such design is also inherent to the greatest degree in the concept of EVT. All beams in EVT are generated in a common electron gun. Then, they are bunched in RF cavities as in a klystron. The energy is transferred from the drive bunches to the accelerated bunch in the accelerating structure. Each cavity of the structure is coupled to all beams, but the cavities are not coupled one to another.

Basic difference from the concept quoted above [2] is that axes of all beams are parallel straight lines and that for beams focusing a homogeneous magnetic field of a solenoid is used. The cavities in EVT are inductively detuned, having the resonant frequencies of their working modes being higher than the operating frequency. As a result, the phase angle between the gap voltage of the cavities and the fundamental harmonic of the drive beam current is close to 90°, as against conditions for the accelerated beam where the phase angle between accelerating gap voltage and a harmonic of a current is close to zero. This operating regime allows one to achieve the desired value of the accelerating field. The most important advantage of using inductively tuned cavities is effective longitudinal bunch focusing, which is exerted by the cavity RF fields of the drive bunches. The drive beam-lets in EVT are weakly relativistic. Therefore, synchronous energy transfer from the drive beams to the accelerated beam is achieved by correct choices of distances Δz between the adjacent cavity gaps. A similar condition, of two-beam acceleration in inductive tuned cavity, is considered by Kazakov et al. [5], where, in contrast to EVT, the authors have placed the drive beam and the accelerated beam on the same axis. Dolbilov G has discussed a two-beam accelerator of protons, where the use of inductive tuned cavities for an electron drive beam is considered [6, 7]. The accelerated beams and the drive beams move there in opposite directions in order to maintain the condition of synchronization.

Preliminary results of numerical simulations using the known and reliable code MAGIC [8] are presented for an EVT prototype, which operates in S-band, where acceleration up to 1 MeV was predicted at efficiency of 66% [9]. A project version of an EVT accelerator operating at L-band, in which a 6-A, 110-kV beam is accelerated to 2 MeV with an overall efficiency of 60%, is presented below. The further development of the EVT concept is based on a principle of two-stage acceleration, where an ensemble of the drive beam-lets is consisting of two groups. At the first stage, the first group of drive beam-lets transfers their energy to the second group of drive beam-lets. At the second stage, the second group of drive beam-lets transfers their energy to the accelerated beam. Such configuration allows a transformation ratio and energy of the accelerated beam to be increased considerably. Numerical simulations predict acceleration of an initial 1 A, 60 keV beam up to energy of 4.3 MeV at efficiency of 22%. The use of a novel view on a Depressed Collector (DC) for a spent drive beam, where the DC is considered as a

http://dx.doi.org/10.5772/intechopen.70956

separator of a spectrum of particles, increases efficiency in the first two EVT projects up to 74 and 68%, respectively. Numerical results are shown in Figures and Tables.

A positive feature of the EVT concept is that the accelerator does not require an external high power RF-source, but only a 60–110-kV pulsed source for operation. The duty cycle for the device will be easily adjusted via the pulse duty cycle of the power supply. The absence of an RF-source, utilization of a relatively low-voltage pulsed power supply to drive the machine, and the compact size of the device would ensure a relatively light weight and highly versatile applied accelerators.

2. EVT configuration

The schematic representation of an EVT accelerator is shown in **Figure 1**, where the accelerating structure is pop up.

An electron gun, a magnetic focusing system and a RF buncher will be provided below in the description of specific projects of EVTs. **Figure 1** (right) provides an example of the accelerating cavity. The operating mode is TM_{020}. An accelerated beam is located in the centre, and a drive beam is located on the periphery, at a peak value of an electric field. The drive beam consists of six beam-lets in the case shown. An additional passive ring-shaped bunching cavity with the fundamental TM_{010} mode is located in a long drift tube. Synchronous energy transfer from the drive beams to the accelerated beam can be achieved through correct choices of distances Δz_1 and Δz_2 between gaps of adjacent accelerating cavities.

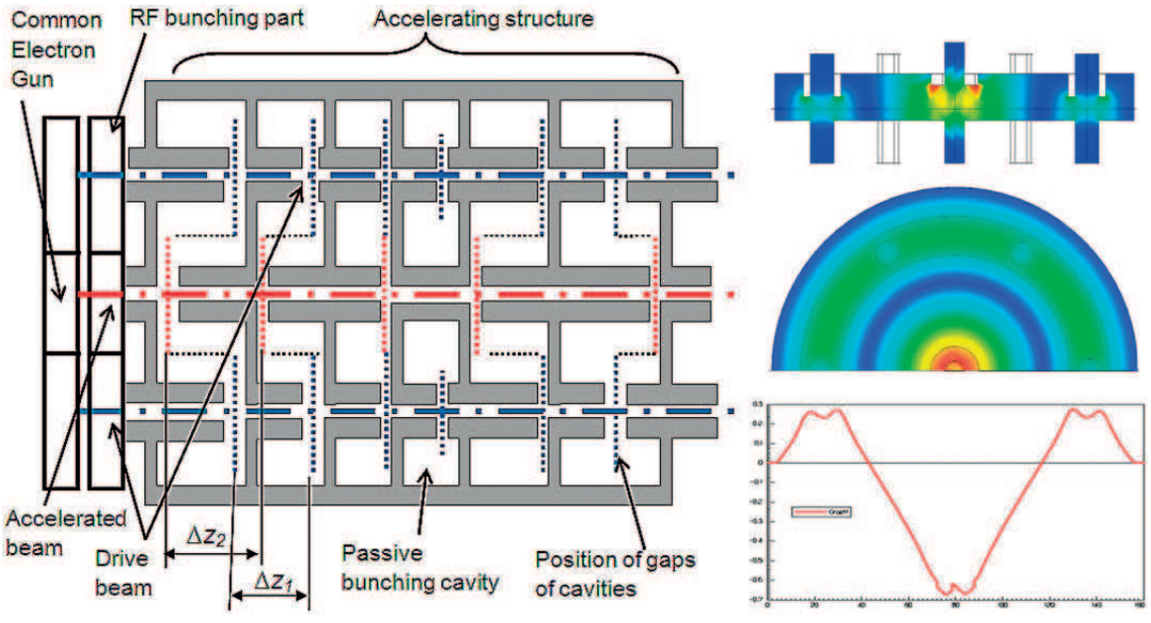

Figure 1. Schematic representation of an EVT (left); shape of the accelerating cavity and electric field E_z along x-axis (right).

3. Scientific and technical justification of the EVT concept

It is known that a field $\mathbf{E}(\mathbf{r},t)$ in a volume Ω of a cavity generated by a beam with a current density $\mathbf{J}(\mathbf{r},t)$ can be presented as eigenmode expansion: $\mathbf{E}(\mathbf{r},t)=\sum_\lambda e_\lambda(t)\cdot\mathbf{E}_\lambda(\mathbf{r})$, where eigen vectors $\mathbf{E}_\lambda(\mathbf{r})$ are functions of coordinate $\mathbf{r}$ that are normalized by energy of the cavity as follows:

$$W_\lambda=\frac{\varepsilon_0}{2}\int_\Omega|\mathbf{E}_\lambda(\mathbf{r})|^2d\Omega. \tag{1}$$

A time-dependent multiplier $e_\lambda(t)$ is the solution of the equation of oscillator with the second member, Eq. (2):

$$\frac{d^2e_\lambda}{dt^2}+\frac{\omega_\lambda}{Q_\lambda}\frac{de_\lambda}{dt}+\omega_\lambda^2e_\lambda=-\frac{1}{2W_\lambda}\frac{d}{dt}\left(\int_\Omega\dot{\mathbf{J}}\cdot\mathbf{E}_\lambda d\Omega\right) \tag{2}$$

Let's express Eq. (2) in a complex form and consider one of the eigenmodes only, having frequency ω_0, replacing: $e_\lambda(t)\rightarrow\dot{e}_0\cdot\exp(i\omega t)$, $\mathbf{J}(\mathbf{r},t)\rightarrow\mathbf{J}(\mathbf{r})\exp(i\omega t)$. It gives

$$\dot{e}_0=\frac{i\cdot\omega}{\omega^2-\omega_0^2-i\cdot\omega\omega_0/Q_0}\cdot\frac{1}{2W_0}\int_\Omega\dot{\mathbf{J}}(\mathbf{r})\mathbf{E}_0(\mathbf{r})d\Omega \tag{3}$$

Other terms of expansion generated by the beam current will have small values at high quality Q_0 of the cavity and at $\omega\approx\omega_O$, and they will not be taken into account. Eqs. (2) and (3) are the most general expressions for determination of fields in cavities [10]. As it takes place $\omega\approx\omega_O$, the equation Eq. (3) can be rewritten as:

$$\dot{e}_0=\exp(i\varphi)\frac{Q_0}{\sqrt{1+\xi_0^2}}\cdot\frac{1}{2\omega W_0}\int_\Omega\dot{\mathbf{J}}\cdot\mathbf{E}_0d\Omega \tag{4}$$

where ξ_0 is a relative detuning:

$$\begin{cases}\xi_0=Q_0\dfrac{\omega^2-\omega_0^2}{\omega\omega_0}\approx\dfrac{2Q_0\Delta\omega_0}{\omega}\\ \Delta\omega_0=\omega-\omega_0\\ \varphi=\tan^{-1}(-\xi_0)\end{cases} \tag{5}$$

Practically, the cavity is described via integral characteristics, such as geometric impedance of drive gap (index 1) and accelerated gap (index 2):

$$\rho_1=(R/Q)_1,\ \rho_2=(R/Q)_2; \tag{6}$$

circuit current $\dot{I}_1$ of the drive gap and circuit current $\dot{I}_2$ of the accelerating gap equal to

http://dx.doi.org/10.5772/intechopen.70956

$$\dot{I}_1 = \exp(i\varphi_1) T_{G1} \cdot 2F_{B1} I_{01}, \qquad \dot{I}_2 = \exp(i\varphi_2) T_{G2} \cdot 2F_{B2} I_{02}; \tag{7}$$

RF beam currents:

$$I_{\mathrm{RF1}} = 2F_{B1} I_{01}, \qquad I_{\mathrm{RF2}} = 2F_{B2} I_{02}; \tag{8}$$

voltage $\dot{\boldsymbol{V}}_1$ of the drive gap along axis z_1 and voltage $\dot{\boldsymbol{V}}_2$ of the accelerating gap along axis z_2:

$$\dot{\boldsymbol{V}}_1 = \dot{e}_0 V_1 = \dot{e}_0 \int_{z_1} E_0(z) dz, \quad \dot{\boldsymbol{V}}_2 = \dot{e}_0 V_2 = \dot{e}_0 \int_{z_2} E_0(z) dz \tag{9}$$

where: φ_1 and φ_2 are phase angles; T_{G1}, T_{G2} are transit time factors of the drive and accelerating gaps, respectively; F_{B1}, F_{B2} are form-factors of bunches; I_{01}, I_{02} are average drive beam currents of the drive and accelerated beams.

For relativistic beams, when it is possible to neglect relative moving of particles inside a bunch, and taking into account that the integral on the second member of Eq. (2) is not equal to zero in gap 1 and gap 2 only where beam currents exist, the Eq. (2) is rewritten as follows:

$$\dot{e}_0 = \exp(i\varphi) \frac{Q_0}{\sqrt{1+\xi_0^2}} \cdot \frac{1}{2\omega W_0} \left(\dot{\boldsymbol{I}}_1 V_1 + \dot{\boldsymbol{I}}_2 V_2 \right). \tag{10}$$

Let us add in relationships under consideration

$$K_V = V_2 / V_1 = \sqrt{\rho_2 / \rho_1}, \tag{11}$$

following from: $2\omega W_0 = V_1^2 / \rho_1 = V_2^2 / \rho_2$.

The description of the equivalent circuit for a case of interaction of relativistic beams with the cavity is

$$\dot{\boldsymbol{V}}_1 = \exp(i\varphi) \cdot \frac{Q_0 \cdot \rho_1}{\sqrt{1+\xi_0^2}} \cdot \left(\dot{\boldsymbol{I}}_1 + K_V \dot{\boldsymbol{I}}_2 \right) = Z_C \cdot \dot{\boldsymbol{I}} \tag{12}$$

$$\dot{\boldsymbol{V}}_2 = -K_V \dot{\boldsymbol{V}}_1 \tag{13}$$

where Z_C is impedance of the drive gap, φ is a phase angle between gap voltage $\dot{\boldsymbol{V}}_1$ and equivalent circuit current $\dot{\boldsymbol{I}}$. Eq. (13) shows properties of the chosen operating eigenmode of a cavity when phases of fields in accelerating and drive gaps are shifted by angle π.

At interaction of a cavity with low relativistic beam it is necessary to consider also beam-loading effect or a beam admittance $Y_B = G_B + i \cdot B_B$. Therefore, Eq. (12) is revised as

$$\dot{\boldsymbol{V}}_1 = \frac{1}{1/Z_C + Y_B} \cdot \left(\dot{\boldsymbol{I}}_1 + K_V \dot{\boldsymbol{I}}_2 \right) \tag{14}$$

Let's set out well-known analytical formulas for a rectangular bunch with angular length ψ_B and for the flat cavity gap having a transit time angle ψ_C:

$$T_C = \frac{\sin(\psi_C/2)}{\psi_C/2}; F_B = \frac{\sin(\psi_B/2)}{\psi_B/2}; \tag{15}$$

$$G_B = \frac{I_0}{V_B} \cdot \frac{1}{2} T_G^2 \left(1 - \frac{\psi_C}{2} \operatorname{ctan} \frac{\psi_C}{2}\right); B_B = \frac{I_0}{V_B} \cdot \frac{\sin\psi_C - (1 + \cos\psi_C)\psi_C/2}{\psi_C^2}, \tag{16}$$

where I_0 is an average beam current, V_B is an average beam voltage in the corresponding gap (drive or accelerating), T_G is the corresponding transit time factor and F_B is a form-factor of the corresponding beam.

3.1. Conditions for preset drive bunching maintenance

As it is known, a bunching cavity has inductive detuning, i.e. $\omega < \omega_0$, at which the phase angle between a gap voltage and an equivalent current of a cavity circuit becomes close to $\pi/2$. **Figure 2** shows mutual position of bunches, currents and gap voltages on a phase plane in an accelerating cavity. The phase position of a head $\dot{H}_{head}$ and tail $\dot{T}_{tail}$ of a drive bunch is shown here, too. Let's notice, that complex RF beam current $\dot{I}_{RF1}$ is displaced at angle π relative to the circuit current $\dot{I}_1$.

3.2. An impedance of the drive gap loaded with the accelerated beam

As it is evidently from **Figure 2**, suitable conditions for an accelerating cavity shall be as follows: $\varphi \to \pi/2$, $\exp(i\varphi) \approx \boldsymbol{i}$. It is the chosen phase of drive current: $\varphi_1 = 0$. The phase of the accelerated beam current equal to $\varphi_2 \approx -\pi/2$ provides a bunch being in the electric field close

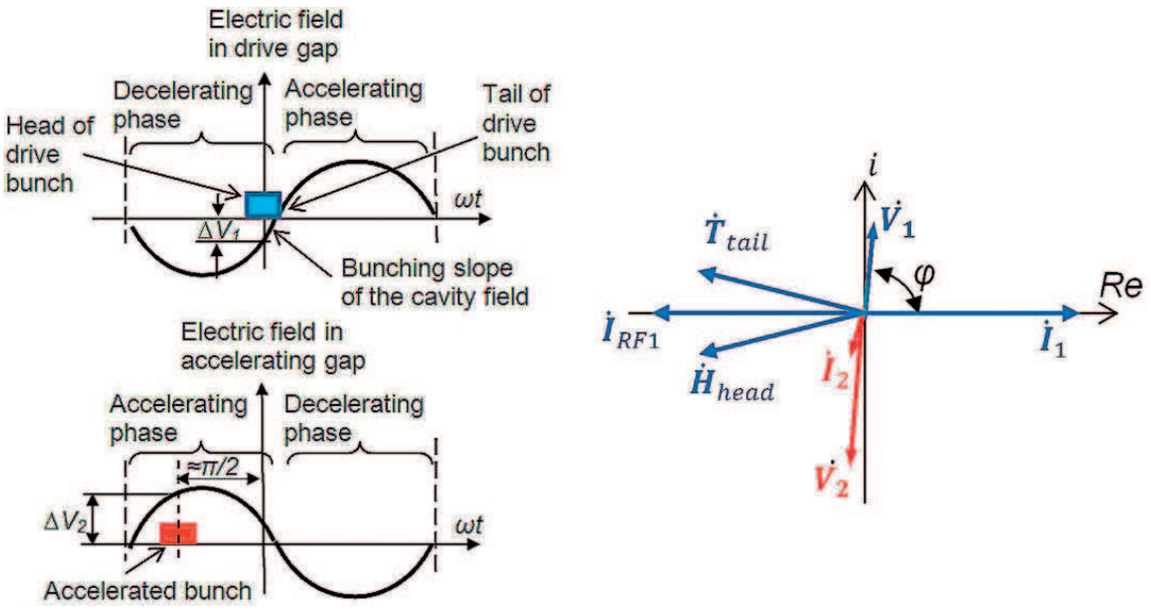

Figure 2. Electric field in cavity gaps (left) and position of complex values on the phase plane (right), providing phase focusing of a drive bunch and acceleration of the beam.

to the peak value, i.e. $\dot{I}_1 = I_1$ and $\dot{I}_2 = -i \cdot I_2$. Thus, using Eqs. (12) and (13), the required impedance of the loaded drive gap is

$$Z_1 = \frac{\dot{V}_1}{\dot{I}_1} = \frac{Q_0 \cdot \rho_1}{\sqrt{1+\xi_0^2}} \left(\frac{K_V}{K_{Tr}} + i \right) \tag{17}$$

where $K_{Tr} = I_1/I_2$ is a transformation ratio. An impedance of the accelerating gap is similarly found:

$$Z_2 = \frac{\dot{V}_2}{\dot{I}_2} = \frac{Q_0 \cdot \rho_1}{\sqrt{1+\xi_0^2}} \left(K_V K_{Tr} - i K_V^2 \right) \tag{18}$$

On the other hand for the equivalent circuit of the cavity the impedance Z_1 is given as:

$$Z_1 = r + i \cdot x = \frac{Q_{load} \cdot \rho_1}{1+\xi_{load}^2} (1 - i \cdot \xi_{load}) \tag{19}$$

where Q_{load} and

$$\xi_{load} \approx 2 Q_{load} \Delta\omega_{load}/\omega \tag{20}$$

are parameters of the equivalent loaded cavity circuit. Equating the real and imaginary parts of Eqs. (18) and (19), the loading quality Q_{load} and relative detuning ξ_{load} can be represented as follows:

$$\begin{cases} Q_{load} = \dfrac{Q_0}{\sqrt{1+\xi_0^2}} \dfrac{K_{Tr}}{K_V} \left(1 + \dfrac{K_V^2}{K_{Tr}^2} \right) = \dfrac{Q_0}{\sqrt{1+\xi_0^2}} \cdot \dfrac{K_{Tr}}{K_V} \\ \xi_{load} = -\dfrac{K_{Tr}}{K_V} \end{cases} \tag{21}$$

Considering Eq. (21) together with Eq. (20) leads to:

$$\frac{\Delta\omega_{load}}{\omega} = -\frac{\sqrt{1+\xi_0^2}}{2Q_0} \cdot \frac{1}{1 + K_V^2/K_{Tr}^2} \approx -\frac{|\Delta\omega_0|}{\omega} \tag{22}$$

where a high value of detuning $\Delta\omega_0$ is suggested, which results in $\sqrt{1+\xi_0^2} \approx |\xi_0|$. In addition, it is assumed that the transformation ratio is large enough, i.e., $K_V^2/K_{Tr}^2 \ll 1$. For example, $K_V \approx 2$, $K_{Tr} \approx 20$, $\Delta\omega_0/\omega \approx 10^{-3}$, $Q_0 \approx 8000$, $\xi_0 \approx 16$.

Eq. (22) shows that loading of the accelerated beam practically does not change the imaginary part of the impedance of the cavity, and, thus, it is possible to model loading as a certain

equivalent external load quality. This feature is used below in the description of numerical model, see Section 4.

3.3. Voltage transformation ratio

Let's find the voltage ΔV_{B1} lost by the drive beam and the voltage ΔV_{B2} added by the accelerated beam, which are connected to a voltage ΔV_1 of the drive gap and a voltage ΔV_2 of an accelerating gap as assigned at the corresponding moment of time (see **Figure 2**):

$$\Delta V_{B1} \approx T_{G1}\Delta V_1, \quad \Delta V_{B2} \approx T_{G2}\Delta V_2 \tag{23}$$

where transit-time factors T_{G1}, T_{G2} are determined the same as in Eq. (7). Let us find voltages ΔV_1 and ΔV_2 using Eqs. (12) and (13) as follows:

$$\begin{cases} \Delta V_1 = \mathcal{R}e(Z_1)\cdot I_1 = \dfrac{Q_0\sqrt{\rho_1\rho_2}}{\sqrt{1+\xi_0^2}}\cdot I_2 \\ \Delta V_2 = \mathcal{R}e(Z_2)\cdot I_2 = \dfrac{Q_0\sqrt{\rho_1\rho_2}}{\sqrt{1+\xi_0^2}}\cdot I_1 \end{cases} \tag{24}$$

where the transformation ratio K_{Tr} is:

$$K_{Tr} = \frac{I_1}{I_2} = \frac{\Delta V_2}{\Delta V_1} \tag{25}$$

In view of Eqs. (7), (8), and (23), the transformation ratio can be written through the RF beam currents as:

$$K_{\mathrm{Tr}} = \frac{I_{\mathrm{RF1}}}{I_{\mathrm{RF2}}} \approx \frac{\Delta V_{B2}}{\Delta V_{B1}}, \tag{26}$$

or, at a high value of transit time factors $T_G \to 1$, Eq. (26) can be written as

$$K_{\mathrm{Tr}} = \frac{I_{01}}{I_{02}}, \tag{27}$$

where I_0 is the average current of the corresponding beam. It reflects the law of conservation of energy for the idealized conditions applied in the beginning of section 3.3 and corresponding to small resistive loss in a cavity. In view of losses it is resulted:

$$K_{Tr} = \frac{I_1}{I_2} = \frac{\Delta V_2}{\Delta V_1}\cdot\frac{1}{\eta_B} \tag{28}$$

where η_B is efficiency of power transfer, defined in the Section 3.4.

3.4. Efficiency of power transfer between beams and other parameters of the EVT

From conservation of energy, the efficiency of power transfer from one beam to another can be estimated as:

$$\eta_B = \frac{\Delta V_2 I_2}{\Delta V_2 I_2 + V_2^2/2R_{s2}} \tag{29}$$

where $R_{s2} = Q_0 \cdot \rho_2$ is the shunt impedance of the accelerating gap. For achieving a high efficiency of energy transfer, it is important to have a large enough current I_2 of the accelerated beam, i.e. $I_2 \gg V_2/2R_{s2}$.

Based on the above consideration and **Figure 2**, it can see that in order to reach the effective bunching of drive beam, with an angle between the current $\dot{\boldsymbol{I}}_1$ and the voltage $\dot{\boldsymbol{V}}_1$ close to $\pi/2$, two conditions shall be satisfied. The first is to have a large enough value of the cavity detuning $\Delta\omega_0$; the second is $I_1/K_V \gg I_2$. The angle between $\dot{\boldsymbol{I}}_1$ and $\dot{\boldsymbol{I}}_2$ should be close to $\pi/2$ for effective acceleration since the accelerated bunch should pass through an accelerating gap at the time when the voltage on the gap is near its maximum. Thus, conditions

$$I_1/K_V \gg I_2 \gg V_2/2R_s \tag{30}$$

are the necessary factors of effective performance of the EVT, which are readily achieved when multiple drive beam-lets are used. For example, $I_1 = 60\ A$, $K_V = 2$, $I_2 = 3\ A$, $\Delta V_2 = 80\ kV$, $V_2 = 100\ kV$, $Q_0 \approx 8000$, $\rho_2 = 60\ ohm$, $\eta_B = 0.95$.

We define the efficiency η of the accelerator as a ratio of the power of the accelerated beam at the EVT output to the total beam power in the gun, namely:

$$\eta = \frac{P_{Accel}}{I_{Gun} V_{Gun}} \tag{31}$$

where I_{Gun} is the total current of the gun, and V_{Gun} is the gun voltage. The high EVT efficiency is confirmed by the results of numerical simulations, as shown in **Table 1**.

We define a voltage gain factor to be a ratio of the voltage of the accelerated beam at the EVT output (the final beam energy) to the gun voltage. It is:

$$K_{EVT} = V_{Accel}/V_{Gun} \approx 1 + K_{Tr} \cdot \eta \tag{32}$$

where η and K_{EVT} are shown in the **Table 1**, as a result of numerical simulations.

3.5. Condition of synchronization and phasing of bunches

The drive beam-lets in the EVT are essentially low relativistic. Therefore, a synchronous energy transfer from the drive beams to the accelerated beam is achieved through correct choices of distances Δz between the adjacent accelerating cavities gaps. In case of equality of distances between gaps shown in the **Figure 1**, a condition of synchronism is as follows:

$$\Delta z = \Delta z_1 = \Delta z_2 = \frac{2\pi c}{\omega} \cdot \frac{\beta_1 \beta_2}{\beta_1 - \beta_2} \tag{33}$$

where $\beta_1 c$ and $\beta_2 c$ are velocities of the drive and accelerated bunches in space Δz between cavities gaps. Phasing capabilities considerably extend if distances Δz_1 and Δz_2 between a gaps of adjacent cavities are not equal to each other. More general Eq. (34) is corresponding to this case:

$$\frac{\Delta z_1}{\beta_1} - \frac{\Delta z_2}{\beta_2} = N \cdot \lambda; \quad N = 0; 1; 2; \ldots; \quad \lambda = 2\pi c/\omega \tag{34}$$

It is supposed to use RF bunchers of klystron type for generation of drive bunches. Further bunches should be decelerated in cavities, gradually giving the energy to the accelerated bunches. There is a reasonable question for how long the drive bunches can keep their form

Multi-beam linear accelerator	**S-band**	**L-band**	
Operating frequency, *F*	2856	1300	MHz
Voltage of common electron gun	60	110	kV
Output energy of accelerated beam	1.1	2	MeV
Total gun current of drive beam	72	180	A
Gun current of accelerated beam	3	6	A
Focusing magnetic field in solenoid	800	1000	G
Energy spread of accelerated beam	±10	±10	%
Micro-perveance of one drive beam-let	0.816	0.82	$\mu A/V^{3/2}$
Transmission of drive beam	0.99	0.99	
Transmission of accelerated beam	0.90	0.87	
Transformation ratio	24	30	
Voltage gain factor	≈18	≈18	
Typical R/Q factor of accelerating gap	58	54	Ω
Typical cavity detuning, $\Delta F = F_0 - F$	8 ÷ 12	7	MHz
Typical K_V factor of gaps of cavity (Eq. 11)	4.5	5	
Efficiency of transfer of power (Eq. 29)	94	97	%
Number of beam-lets of drive beam	6	6	
Number of cavities of RF bunchers	4	4	
Number of accelerating cavities	14	12	
Number of passive bunching cavities	1	7	
Length of RF part of accelerator	0.79	2.4	m
Efficiency of accelerator EVT	≈66	≈60	%
Efficiency of EVT with DC for drive beam	72	66	%

Table 1. The simulated parameters of the S-band and L-band linear accelerators EVT.

http://dx.doi.org/10.5772/intechopen.70956

and phase length. Results of 2D simulations show long enough conservation of the generated bunch (see below projects of EVT). The similar research confirming these results can be found in [6, 7].

4. Representation of 3D objects via equivalent 2D objects

3D codes have been used for simulation of elements of the EVT (cavities, magnetic system), but for the analysis and optimization of dynamics of ensemble of the interacting beams moving in numerous drift tubes the direct and slow 3D analysis is too intricate problem. Difficulty is aggravated also with necessity of carrying out numerous optimizations.

The drive beam-lets are located on a circle, see **Figure 1** (right), and it can be quite replaced with single equivalent 2D annular beam. It is possible to choose the corresponding width of the ring filled with a beam, providing close values of plasma wave-lengths of 2D and 3D models of the beam. In the same way it is replaced real 3D cavities with equivalent 2D cavities. There are chose parameters (gap, R/Q) of interaction of a 2D beam with equivalent 2D cavities similar to interaction of a 3D beam with 3D cavities. Certainly, such equivalent model does not describe exact dynamics of the drive beam, but reflects quite well the properties of the EVT accelerator and can serve as initial approach. The results of parameter optimization for the EVT accelerators using the 2D code MAGIC [8], are provided in Sections 5–7.

It is obvious that, on the one hand, implementation of a pure annular concept of the drive beam is embarrassing technically, and, on the other hand, the annular model is rather rough to describe dynamics of a set of cylindrical drive beam-lets. This simulation is provided here to illustrate a method of acceleration used in the EVT as it correctly represents interaction of two electron beams without any additional assumptions.

The following, more adequate model is appropriate for description of a 3D problem, which can be named **2 × 2D** model. This model is based on thesis about an impedance of the loaded drive gap considered in Section 3.3 and on the following circumstances:

1. Each of beam-lets and electric RF fields of cavities near to a beam-let can be considered as axially symmetric relative to a local axis of the given beam-let;
2. Parameters of drive beam-lets are identical;
3. Accelerating cavities are weakly loaded, and, therefore, RF fields of cavities are rather close to a field of an operating RF eigenmode. I.e. the loaded quality of a cavity remains high enough. In other words, the RF power circulating in a cavity $P_{RF} = \frac{V_1^2}{2R/Q_1}$ is much higher than power $\Delta P_2 = P_{output2} - P_{input2}$ transferred to the accelerated beam, for example, $Q_{load} = P_{RF}/\Delta P_2 \geq 100$.

According to these points, it is considered a 3D problem as two connected 2D problems, see **Figure 3**. The drive beam goes through the first equivalent 2D cavity, having the R/Q of drive

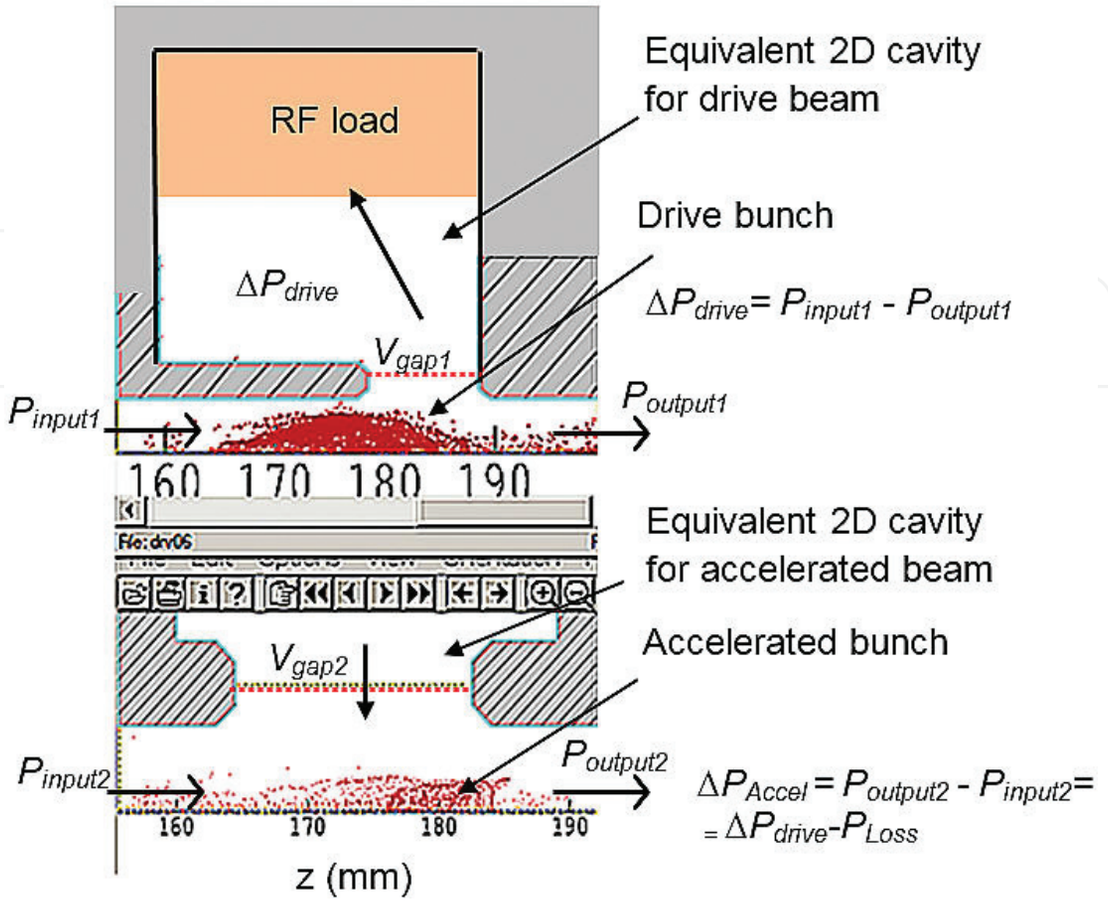

Figure 3. Two 2D cavities, the parameters of which are related via the shown relationships, model processes in a 3D cavity.

gap equal to R/Q of corresponding 3D cavity. This cavity has an RF load in which RF power $P_{load} = \Delta P_{drive}$ is absorbed.

The accelerated beam goes through the second cavity having a gap voltage V_{gap2} and a phase angle φ_{gap2}, which are calculated based on a voltage V_{gap1} on the gap of the cavity 1 for the drive beam and where power of the accelerated beam increases at the value $\Delta P_2 = P_{output2} - P_{input2}$. Positions of gaps of these two equivalent cavities correspond to the position of gaps of the 3D cavity. Combination of these two processes will consist in maintenance of equations:

$$\begin{cases} \Delta P_2 = \Delta P_{accel} = 6 \cdot \Delta P_{drive} - P_{loss} \\ V_{gap2} = K_V V_{gap1} \\ \varphi_{gap2} = \varphi_{gap1} + \pi \end{cases} \tag{35}$$

where $N = 6$ is the number of drive beam-lets, P_{loss} is resistive loss in the 3D cavity. Eq. (35) is carried out by choosing the corresponding conductivity of an external RF load of the first (drive) cavity; the value $K_V = \left(\frac{V_{gap2}}{V_{gap1}}\right)_{3D}$ is defined (see Eq. 11) upon the results of the 3D cavity

http://dx.doi.org/10.5772/intechopen.70956

eigenmode analysis. Numerical simulations using the code MAGIC show fast convergence of the Eq. (35) process. 2–3 iterations are practically enough.

5. Design of S-band 1 MeV linear accelerator EVT

The design of a linear accelerator EVT operating in S-band (F = 2856 MHz) and generating 1 MeV electron beam is presented in this section. One accelerated beam and 6 drive beam-lets are generated by a common electron gun fed from a 60 kV power supply. The magnetic lenses around the gun and two matching lenses ensure formation of beams without ripples in the same way, as it is described in Ref. [3]. Bunches are formed in the bunching section energized by two coherent microwaves via RF couplers. The generated drive beam-lets interact with the accelerated beam in the cavities of the energy transfer section (accelerating structure), with the cavities working at the TM_{020} mode. For a layout of the S-band EVT, please see **Figure 4**.

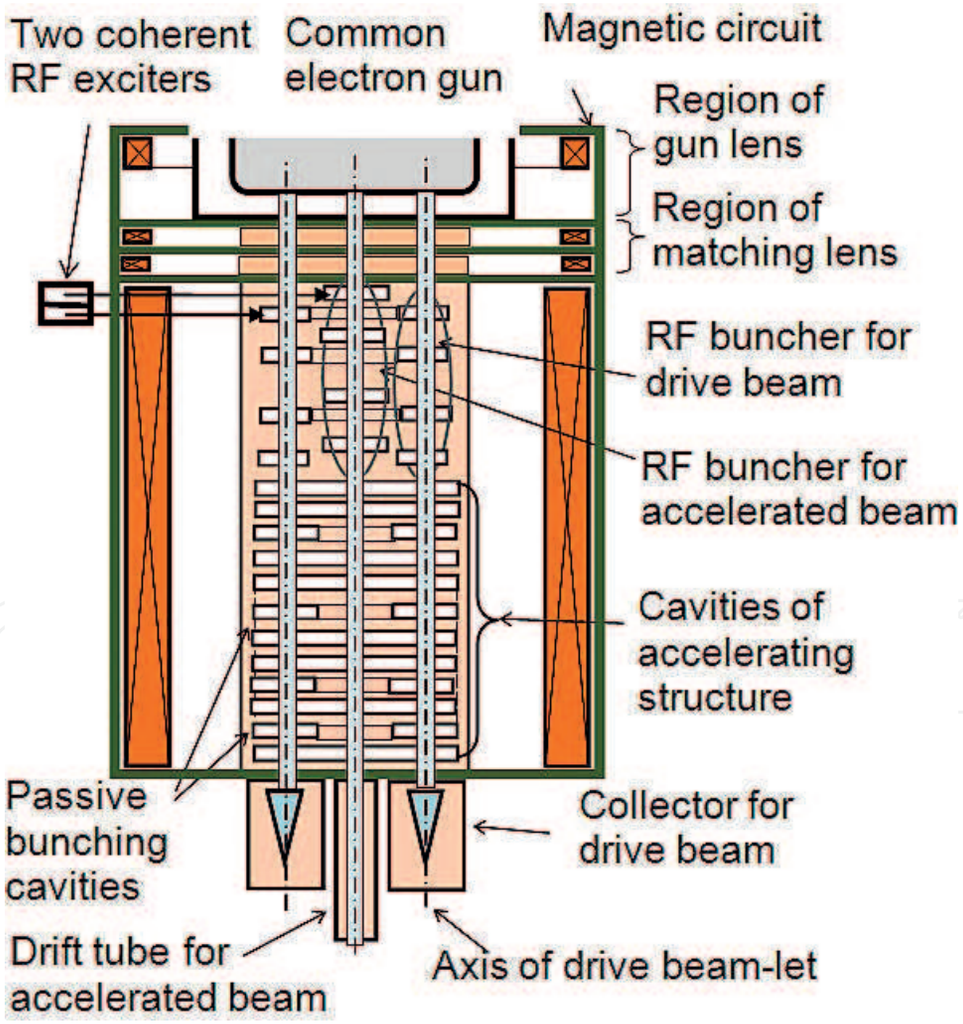

Figure 4. Lay-out of the accelerator EVT.

The results of the initial numerical analysis using code MAGIC are given below in **Table 1**. Two models described above in Section 4 have been applied for the analysis. The models have shown close results. Beam dynamics of the annular model is more evident and results in **Figure 5**. **Figure 6** shows energy distribution of particles of beams in the 1st accelerating cavity ($z > 314$ mm) and at the output of the accelerating structure ($z > 787$ mm). Energy of 1.1 MeV, averaged on the size of a bunch, is achieved. You can see disruption of the spent drive bunches at the accelerator output. The achieved 66% efficiency is twice the best efficiency accessible for the facility consisting of a high power klystron and a high efficient linear accelerator [11].

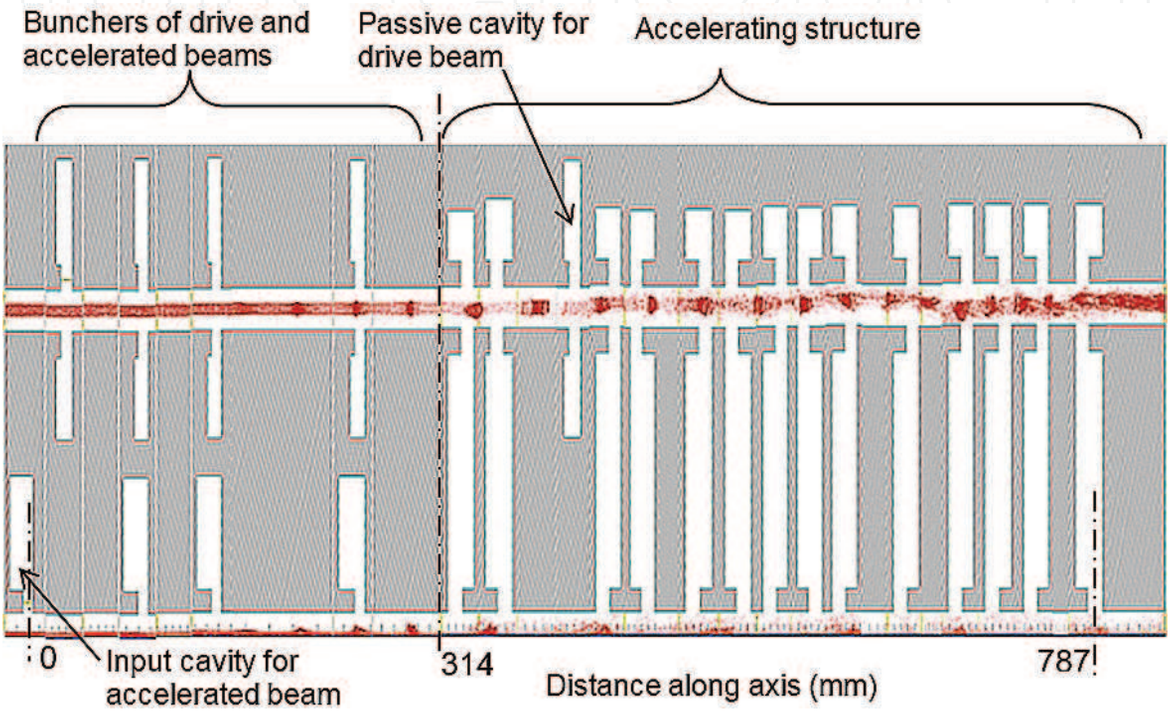

Figure 5. The geometry of a compound RF buncher, accelerating structure and beams dynamics are shown for the S-band EVT.

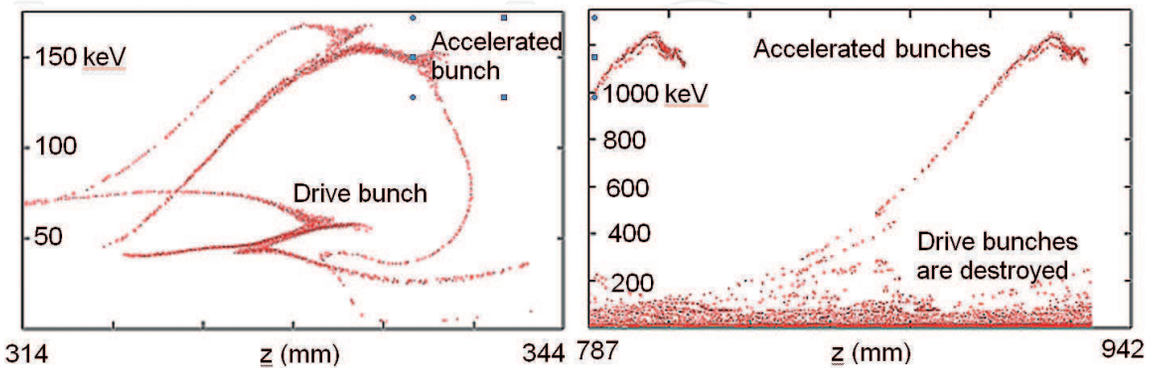

Figure 6. Particle energy distribution in the 1st accelerating cavity (left) and at the output of the accelerating structure (right).

5.1. Features of the multi-beam electron gun

The radius of a ring on which drive beam-lets are located is defined by a frequency and configuration of the cavities (see **Figure 1** (right)). Six cathodes with a current of 12 A are freely

http://dx.doi.org/10.5772/intechopen.70956

located on this radius at the gun voltage 60 kV, **Figure 7**. Clearly, a drive beam-let perveance should not be too high to not interfere with phase stability and synchronization of bunches.

Distance between the drive beam-let cathodes is big enough in comparison with distance between the cathode and anode therefore transverse electrostatic fields on an axis of drive beam-lets are insignificant. Thus the electron optics of each of beam-lets can be quite considered as axial symmetric. **Figure 8** shows the 2D geometry and an example of simulation of a drive beam-let. The double lens around the gun allows obtain the desired profile of the magnetic field to focus the beam-lets and minimize their ripples.

Cells of magnetic lenses are formed by flat iron pole-pieces and system of apertures (see **Figure 4**). Properties of cells for drive beam-lets are identical. The sizes of apertures and distances between

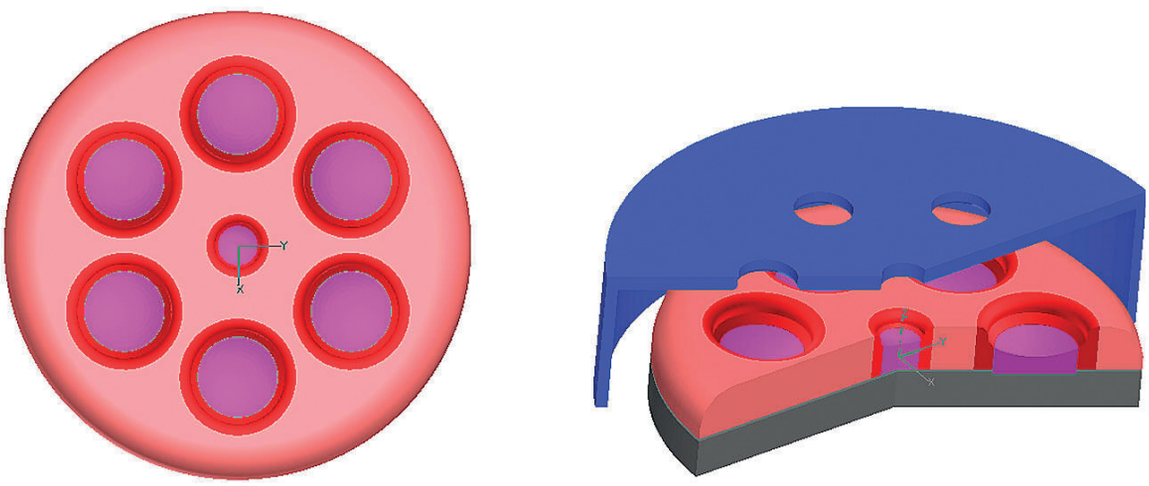

Figure 7. The multi-beam cathode of the electron gun. The peripheral cathodes generate the drive beam-lets, and the central cathode generates the accelerated beam.

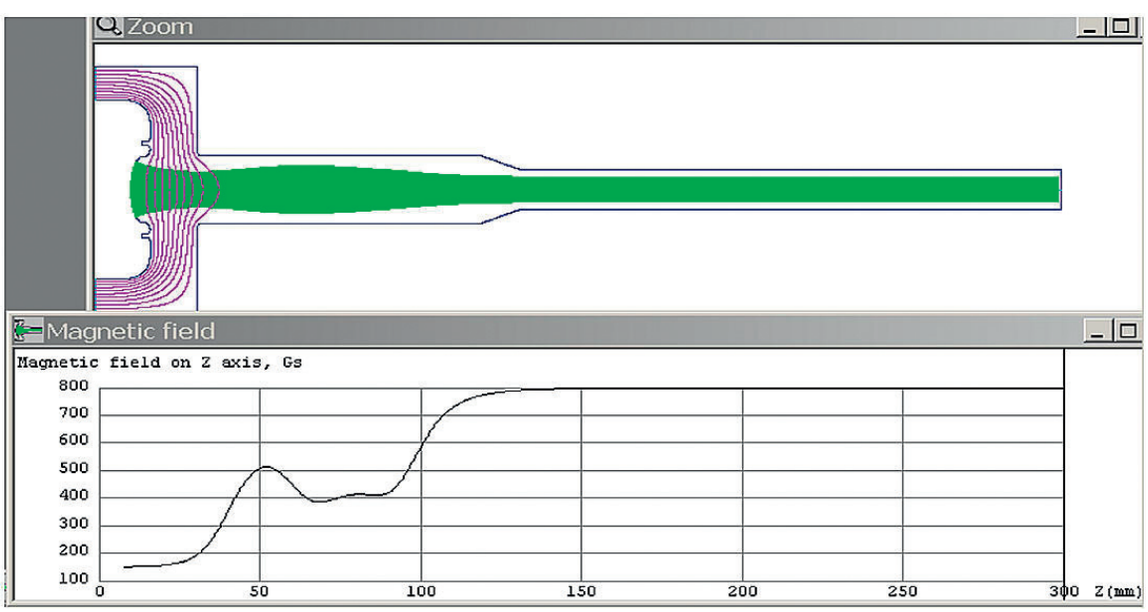

Figure 8. The geometry and an example of 2D simulation of the drive beam-let gun.

them are such that there are no appreciable transverse fields generated on an axis of beam-lets. Thus, the magnetic field quite possesses axial symmetry near the beam-let axis.

6. Specification of L-band 2 MeV linear accelerator EVT

The S-band EVT project has shown achievement of a high efficiency, but has simultaneously shown limited capabilities for an acceleration rate and for a factor of transformation as decay of bunches after $N_{cav} = 15$ cavities has been observed. Numerical results show difficulty of bunch confinement at a voltage of a drive gap $V_{gap1} > \frac{1}{2} V_{gun}$. It results in the following limiting estimated condition:

$$V_{\text{Accel}} < \frac{1}{2} K_V N_{\text{cav}} V_{\text{gun}}, \tag{36}$$

where K_V is from Eq. (11). This estimation is close to observable result $V_{Accel} = 1.1\ MeV$ achieved in the S-band EVT.

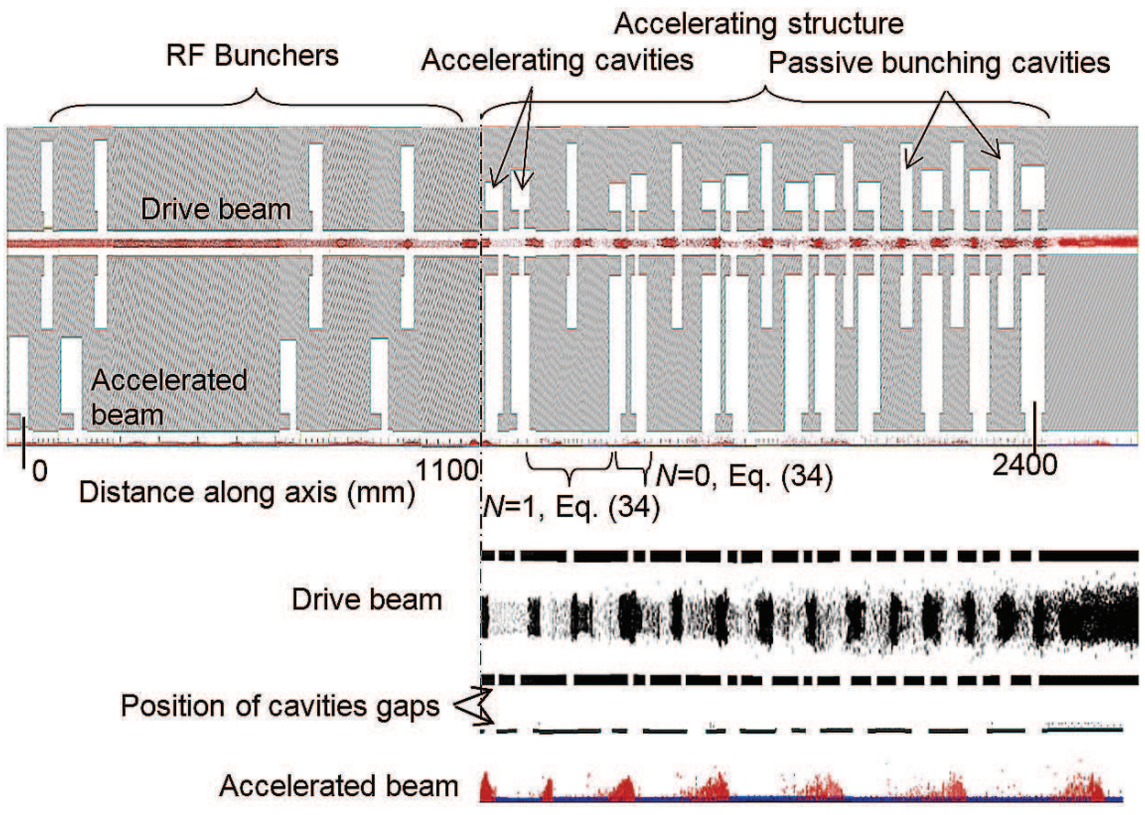

Figure 9. Geometry of the RF structure and the result of numerical simulations are shown for L-band EVT. For more details on the dynamics of the beams, please see below.

http://dx.doi.org/10.5772/intechopen.70956

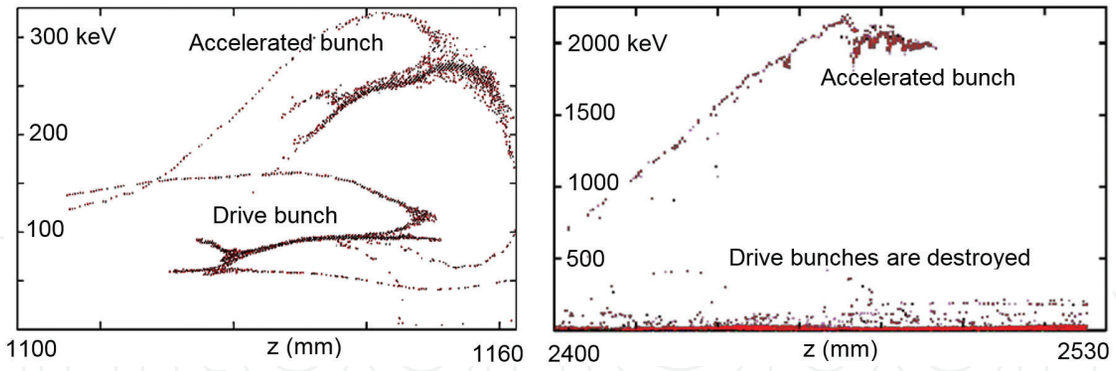

Figure 10. Particle energy distribution at the output of the 1st accelerating cavity (left) and at the output of the accelerator section (right).

Thus, an advance in a path of higher voltage of the gun and a low frequency is meant to increase a voltage of an accelerated beam in the described L-band EVT. Its layout does not differ from **Figure 4**. Numerical simulations have shown feasibility of reaching the energy of the accelerated beam about 2 MeV with efficiency about 60% at a gun voltage equal to 110 kV. More detailed data of the project are submitted in **Table 1**. The accelerating structure includes 12 accelerating cavities and 7 passive cavities (see **Figure 9**). The code MAGIC 2D and both models described in Section 4 have been applied for the analysis. For the results of beam dynamics of the annular model, please see **Figure 9**, too. **Figure 10** shows particle energy distribution.

7. Two-stage multi-beam linear accelerator EVT

The further increase in energy of the accelerated beam will consist in increase in a voltage of a drive beam. It is suggested to consider two-stage acceleration. Let's assume that the set of the drive beam-lets consists of two groups. At the first stage, the first group of drive beam-lets that form drive beam 1 transfer their energy to the second group of beam-lets that form drive beam 2. At the second stage, the second group of drive beam-lets transfers their energy to the accelerated beam. Such configuration is allowed to increase a transformation ratio and energy of the accelerated beam considerably. Preliminary results of numerical simulations of two-stage EVT operating in S-band with a 60 kV gun and generating a 1 A, 4.3 MV beam at its output, with an efficiency of 22%, are presented. See **Figure 12** and **Table 2**.

Figure 11 (left) shows a multi-beam cathode system. 36 peripheral cathodes generate the drive 1 beam-lets, and 6 cathodes generate the drive 2 beam-lets. The central cathode generates the accelerated beam. A rather low perveance (0.41 $\mu A/V^{3/2}$) of drive beam-lets is chosen. It is allowed to simplify the magnetic system and electron optics of the gun. The drive beam is frozen in a homogeneous magnetic field of the focusing solenoid. You can see the presence of ripples having an allowable value in **Figure 11** (right).

MAGIC 2D simulations of beam dynamics were carried out using an annular model of beams and cavities. Please see the results of numerical simulations in **Figures 12–14** and in **Table 2**.

Figure 14 shows particle energy distribution at the accelerator output. For the change in beams energy vs. distance, please see **Figure 15**.

Operating frequency	2856		MHz
Voltage of common electron gun	60		kV
Output energy of accelerated bunch	4.3		MeV
Average energy of accelerated beam	3.6		MeV
Gun current of accelerated beam	1		A
Total gun current of drive beams	252		A
Solenoid magnetic field	1000		G
Length of RF part of accelerator	1.9		m
Transmission of accelerated beam	90		%
Total efficiency of two-stage EVT	≈22		%
Stage	1st	2nd	
Gun current of drive beam	216	36	A
Perveance of drive beam-let	0.41	0.41	$\mu A/V^{3/2}$
Transformation ratio	6	36	
Voltage gain factor of stage	≈3.5	≈21	
Number of drive beam-lets	36	6	
Transmission of drive beam	98	90	%
Efficiency of stage	≈55	≈45	%

Table 2. Simulated parameters of the two-stage EVT.

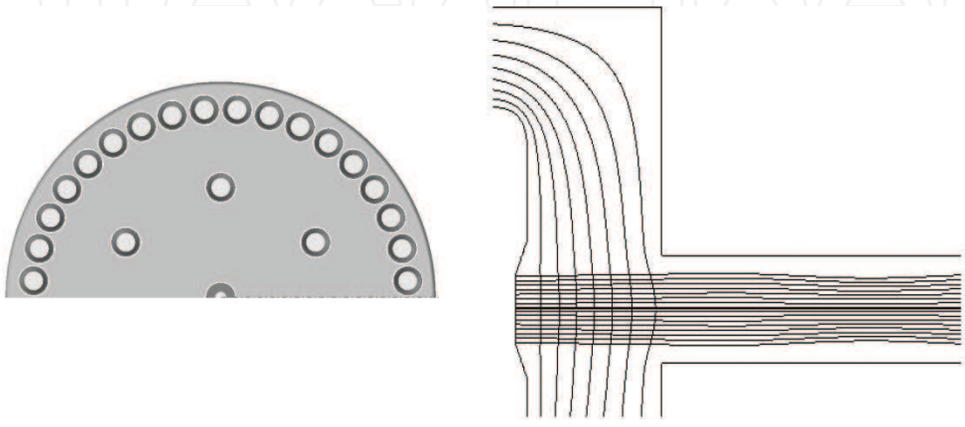

Figure 11. Multi-beam cathode system of the two-stage EVT (left) and an example of 2D simulation of the drive beam-let gun (right).

http://dx.doi.org/10.5772/intechopen.70956

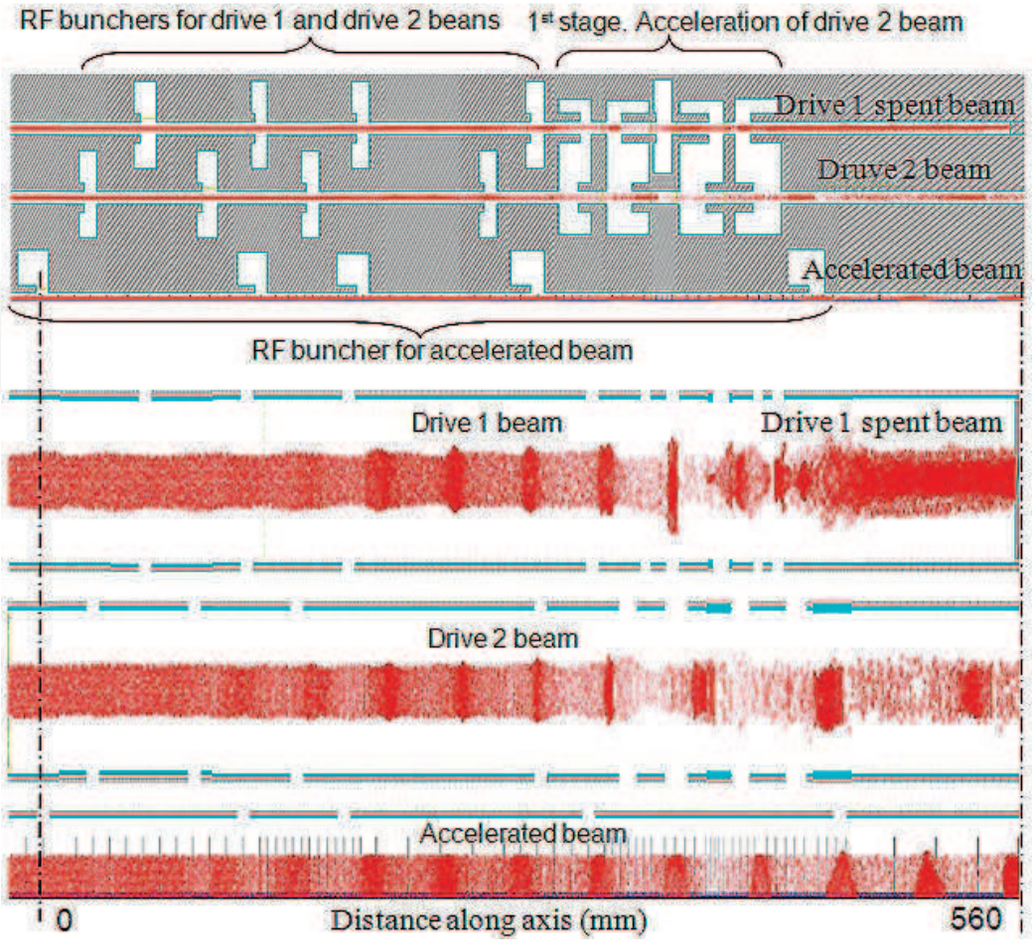

Figure 12. MAGIC 2D results of simulation of beam dynamics in the bunching part and at the 1st stage.

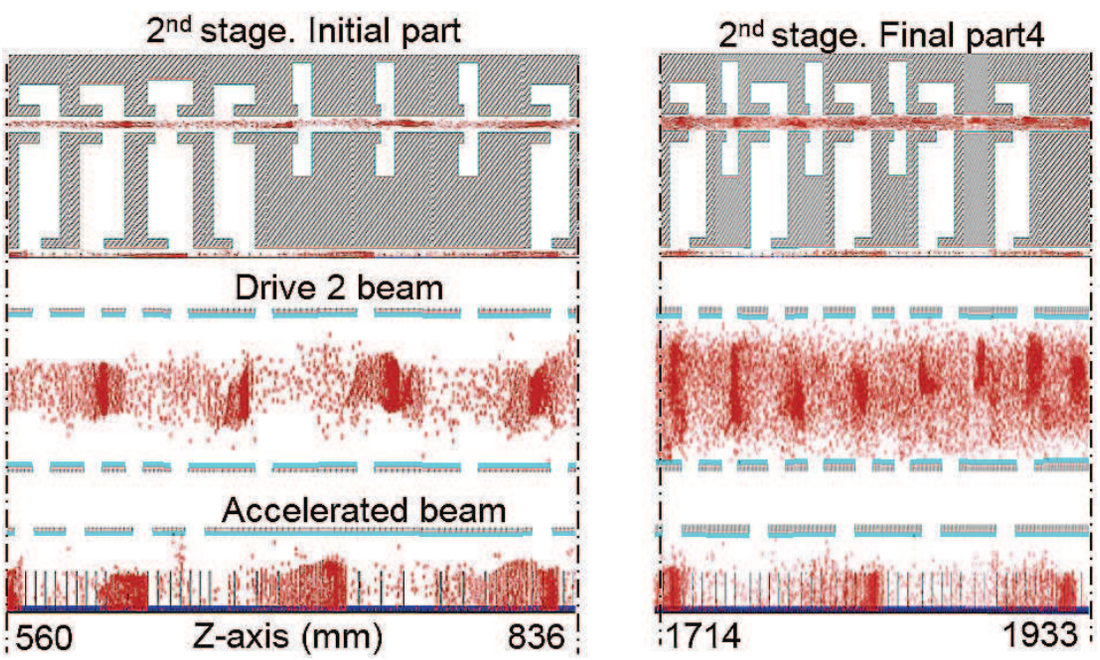

Figure 13. Accelerating structure of 2nd stage. Dynamics of drive 2 and accelerated beams.

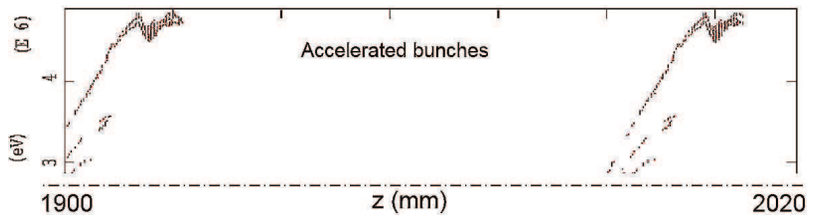

Figure 14. Energy distribution at the output of the two-stage EVT.

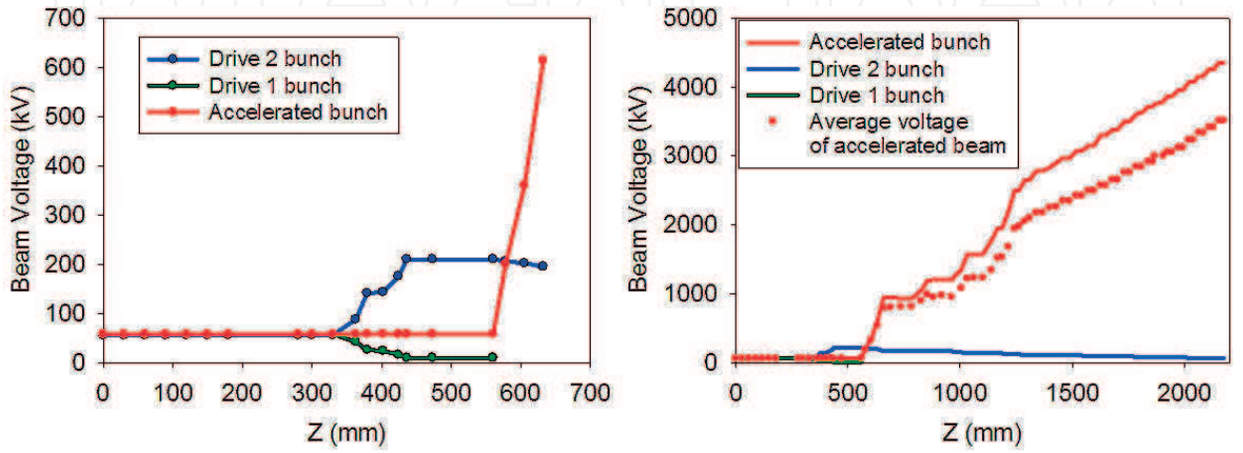

Figure 15. Change of beams voltage along the accelerator axis.

8. Depressed collector (DC) for spent drive beam

The efficiency of 66% achieved in preliminary numerical simulations of the S-band EVT is a rather high value. The further increase in efficiency of the EVT accelerators is possible at the use of a depressed collector. It is suggested considering a novel concept of a DC, which allows theoretical estimation of DC properties. The given concept is based on the thesis of existence of an extremum of the DC efficiency versus DC voltage. The concept does not struggle with the energy distribution of electrons having a place after the device output, but uses properties of energy distribution. Let us name this concept a depressed collector with a spectra separator, DC&SS. The schematic circuit of the tube with a one-stage DC is shown in **Figure 16** (left). **Table 3** shows the basic relationships describing the circuit of the EVT with a DC.

Substituting the above resulted relationships, it is derived the total tube efficiency with a DC:

$$\eta_t = \frac{\eta_e}{1 - (1 - \eta_e)\eta_c} \tag{37}$$

Eq. (36) is well known (see, for example [12]), but we shall regard it now jointly with the presence of an energy spectrum of particles leaving a tube. Variable $I_c = I_c(V_c)$ is remarkable since it is a function of a collector voltage as a consequence of the presence of energy distribution. Our subsequent problem is to study the function $\eta_c(V_c)$ in order to find an extremum at some assumptions concerning the energy distribution $j(V)$, which is normalized on the beam current I_B:

http://dx.doi.org/10.5772/intechopen.70956

$$\int_0^\infty j(V)dV = I_B \tag{38}$$

In the gap of the separator, the beam is divided into low-voltage and high-voltage fractions. The current

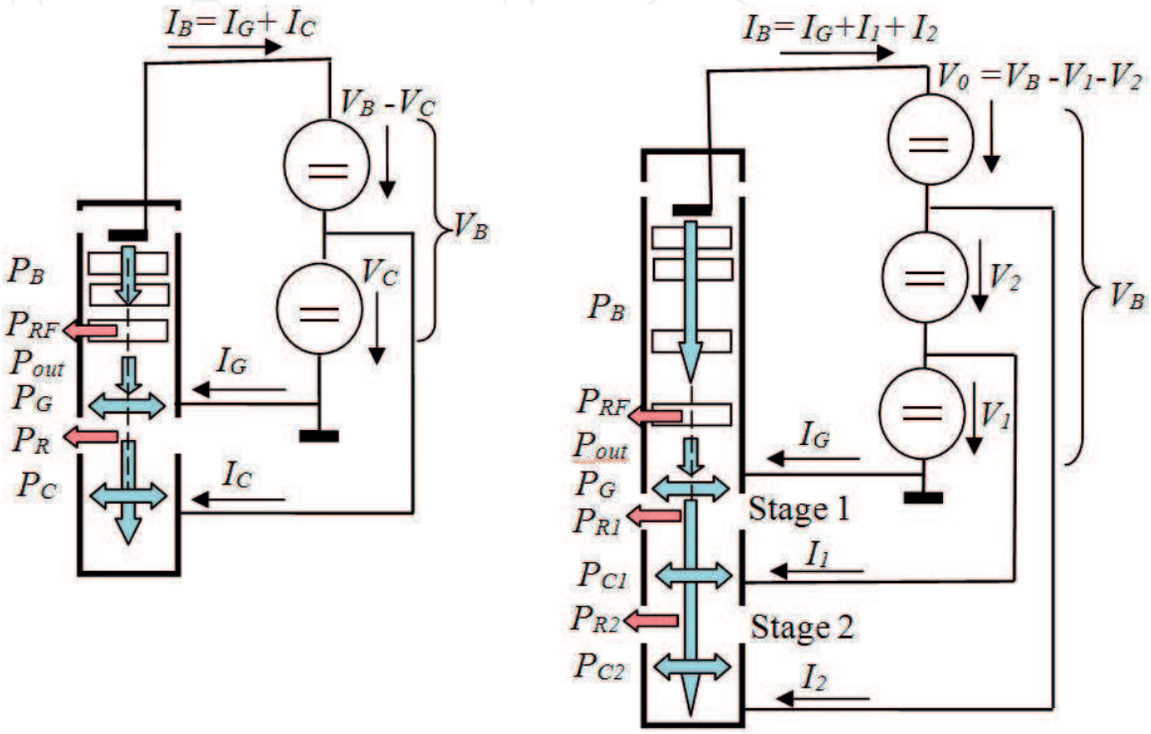

Figure 16. Schematic circuit of a tube with depressed collector. One-stage DC (left); two-stage DC (right).

Beam voltage	V_B
Voltage of stage	V_C, V_1, V_2
Current of potential part of stage	I_C, I_1, I_2
Beam power	$P_B = I_B V_B$
RF power, transfer to accelerated beam	P_{RF}
Loss power in ground part of collector	P_G
Loss power in potential part	P_C, P_{C1}, P_{C2},
EVT electron efficiency	$\eta_e = P_{RF}/P_B$
Beam power at output of tube	$P_{Out} = (1 - \eta_e)P_B$
Recovery power	$P_R = V_C I_C$
Total power generating by high-voltage source	$P_t = V_B I_B - V_C I_C$
Efficiency of depressed collector	$\eta_c = P_R/P_{Out} = V_C I_C/P_{Out}$
Total tube efficiency with DC	$\eta_t = P_{RF}/P_t = P_{RF}/(P_B - V_C I_C)$

Table 3. Notations and relationships describing a DC.

$$I_c(V_c) = \int_{V_c}^{\infty} j(V)dV \tag{39}$$

that has reached the potential part of the collector is the fraction of the current at which $V > V_C$. In the same way, it is written down the equation for the beam power leaving the accelerating structure:

$$P_{out} = \int_0^{\infty} V \cdot j(V)dV \tag{40}$$

Thus, it is evaluated the fundamental formula Eq. (41) for efficiency η_c of a depressed collector included in the DC&SS concept:

$$\eta_c(V_c) = \frac{V_c \int_{V_c}^{\infty} j(V)dV}{\int_0^{\infty} V \cdot j(V)dV} \tag{41}$$

Figure 6 (right) above shows a numerical example of the energy distribution for the spent drive beam of the S-band EVT versus distance along beam axes. **Figure 17** shows the energy distribution of the same beam. The gamma distribution $x \cdot e^{-x}$ (curved line) can serve as a close approximation for numerical distribution.

Thus, let us approximate $j(V)$ by the gamma distribution:

$$j(V) = \frac{I_B}{V_0} x \cdot e^{-x} \tag{42}$$

where $x = V/V_0$, $V_0 = V_B(1 - \eta_e)/2$. Further, it is defined I_c according to Eq. (39):

$I_c(x_c) = I_B \cdot e^{-x_C}(x_C + 1)$, where $x_c = V_c/V_0$, and it is defined P_{out} according to Eq. (40):

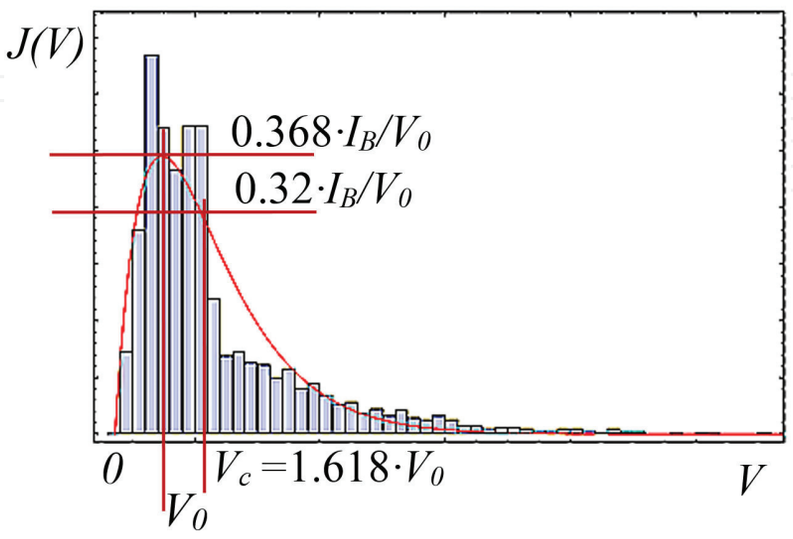

Figure 17. A numerical simulated histogram of particle distribution vs. voltage and an approximating gamma distribution are shown for the S-band EVT.

$$P_{out} = 2I_B V_0 \tag{43}$$

Substituting the found expressions in Eq. (41), it is obtained:

$$\eta_c(x_c) = \frac{1}{2} x_c e^{-x_c}(x_c + 1) \tag{44}$$

The function $\eta_c(x_c)$ has the maximum equal to **0.42** at $x_c = \frac{1+\sqrt{5}}{2} = 1.618$.

Thus, it is derived the collector efficiency and other parameters at the optimum point:

$$\eta_c = 0.42; I_c = 0,519 \cdot I_B; I_G = 0,481 \cdot I_B; V_c = 1.618 \cdot V_0. \tag{45}$$

As an example of the S-band EVT (**Table 1**), one have:

$$V_B = 6 \cdot 10^4; \eta_e = 0.66; V_0 = V_B(1 - \eta_e)/2 = 1.02 \cdot 10^4; V_c = 1.65 \cdot 10^4. \tag{46}$$

The total efficiency (according to Eq. 37) at the optimum point is $\eta_t = 0.77$, which is the upper theoretical limit!

For a DC having m stages i.e. m gaps and consequently m gap voltages (see **Figure 16**), efficiency is as follows:

$$\begin{cases} \eta_t = \dfrac{\eta_e}{1 - (1 - \eta_e)\eta_c} \\ \eta_c = \sum_{n=1}^{m} \eta_n \end{cases} \tag{47}$$

where η_c is DC efficiency in multi-stage case. The collector efficiency η_n of the n^{th} stage is calculated according to the Eq. (41), where the lower limit of integration is equal to potential $U_n = \sum_{i=n}^{m} V_i$ of the given stage concerning the ground. This Eq. (48) defines the concept of a DC&SS in multi-stage case:

$$\eta_n(V_1, V_2, \ldots V_n) = \frac{V_n \int_{U_n}^{\infty} j(V)dV}{\int_0^{\infty} V \cdot j(V)dV} \tag{48}$$

Using the approximation (see Eq. 42) for beam distribution $j(V)$, leads to:

$$\begin{cases} \eta_n = \dfrac{1}{2}\left[x_n \left(1 + \sum_{i=n}^{m} x_i \right) e^{-\sum_{i=n}^{m} x_i} \right] \\ \eta_c = \sum_{n=1}^{m} \eta_n \end{cases} \tag{49}$$

where: $x_i = V_i/V_0$, $x_n = V_n/V_0$, $V_0 = V_B(1 - \eta_e)/2$, V_i is gap voltage of the i^{th} stage, V_B is beam voltage. For a schematic circuit of a tube with a two-stage DC, **Figure 17** (right), the total collector efficiency will be as follows:

$$\eta_c(x_1, x_2) = \eta_1 + \eta_2 = \frac{1}{2}\left[x_1(1+x_1)e^{-x_1} + x_2(1+x_1+x_2)e^{-(x_1+x_2)}\right] \tag{50}$$

The extremum of this function is equal to $\eta_c = 0.586$ at: $x_1 = 1.118$; $x_2 = 1.398$.

At $\eta_e = 0.66$, according to Eq. (37), it will correspond to the total tube efficiency $\eta_t = 0.824$.

Table 4 shows the results of efficiency η_c optimization for a collector that contains one to six stages.

m	x_1	x_2	x_3	x_4	x_5	x_6	η_c
1	1.618						0.420
2	1.118	1.398					0.586
3	0.884	0.941	1.319				0.676
4	0.743	0.732	0.876	1.276			0.734
5	0.648	0.608	0.675	0.841	1.249		0.773
6	0.578	0.526	0.558	0.645	0.819	1.229	0.803

Table 4. The optimization result for the function $\eta_c(x_1, x_2, \ldots)$ via its parameters $x_1, x_2, \ldots$.

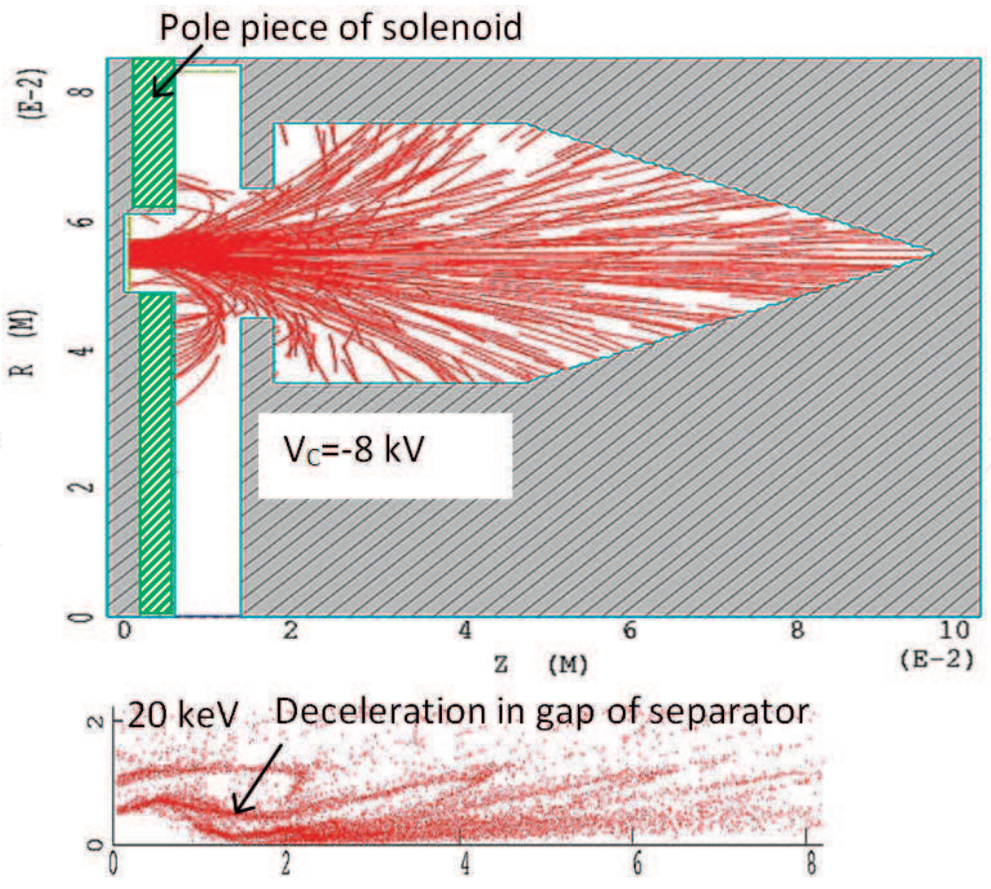

Figure 18. Geometry of a one-stage DC for the S-band EVT. A picture of particles energy is added at the bottom of the figure.

http://dx.doi.org/10.5772/intechopen.70956

The theoretical premise of an increase in efficiency of a device with a multi-stage DC are rather optimistic. However, simulations of beam dynamics in conditions close to real do not show any noticeable increase in the device's efficiency while engineering complexity of such multi-stage DC tangibly increases. Thus, use of a one-stage DC is, perhaps, more preferable in practice.

The analytical treatment described above is rather idealized as it does not include the beam particle movement dynamics; however, it shows parameters to which there can try to approach. The result of initial simulation of a one-stage DC for a spent drive beam of the S-band EVT is shown in **Figure 18**. No special optimization of the DC geometry and the magnetic field shape was carried out. Secondary emission was not taken into consideration either. The annular 2D model of the drive beam has been used.

The results of initial simulations have shown a DC efficiency about 25%, which increases the total efficiency of the S-band EVT up to 72%. It certainly is substantially lower than the idealized theoretical results of the previous section and allows further optimization.

9. Conclusion

Theoretical and numerical research of properties of the linear accelerator EVT has shown that there is sufficient comprehension about it properties. There is no visible vagueness in technical problems. Certainly, the EVT accelerator does not show a record rate of acceleration; however, it shows that to reach a high efficiency of 70% or more is possible. It is much higher than the total efficiency of a klystron loaded with an ordinary linear accelerator. The two-stage configuration of the accelerator considerably increases the transformation ratio, but the accelerator's efficiency decreases; therefore, further optimization of this configuration is preferable. Thus, there are all preconditions in place to proceed with the engineering design.

Author details

Vladimir E. Teryaev

Address all correspondence to: vladimir_teryaev@mail.ru

Budker Institute of Nuclear Physics, Novosibirsk, Russia

References

[1] Corsini R. Two-beam linear colliders – Special issues. In: Proceedings of PAC09; 2009; Vancouver, BC, Canada. IEEE; 2009. pp. 3100-3104

[2] Derbenev Ya S, Lau YY, Gilgenbach RM. Proposal for a novel two-beam accelerators. Physical Review Letters. 1994;**72**(19):3025-3028. http://patents.justia.com/patent/5483122

[3] Teryaev VE, Hirshfield JL, Kazakov S, Yakovlev VP. Low Beam Voltage, 10 MW, L-Band Cluster Klystron. In: Proceedings of PAC09; 2009; Vancouver, Canada. http://accelconf.web.cern.ch/AccelConf/PAC2009/papers/tu5pfp093.pdf

[4] Teryaev VE, Shchelkunov SV, Kazakov SY, Hirshfield JL, Ives RL, Marsden D, Collins G, Karimov R, Jensen R. Compact low-voltage, high-power, multi-beam Klystron for ILC: Initial test results. In: Proceedings of the Division of Particles and Fields; Aug 4–8, 2015; Ann Arbor, MI, USA. http://arxiv.org/abs/1510.06065

[5] Kazakov SY, Kuzikov SV, Jiang Y, Hirshfield JL. High-gradient two-beam accelerator structure. Physical Review Special Topics - Accelerators and Beams. 2010;**13**(7):071303-071301. https://journals.aps.org/prab/abstract/10.1103/PhysRevSTAB.13.071303

[6] Dolbilov GV. Two-beam induction linear collider. In: Proceedings of EPAC 2000; 2000; Vienna, Austria. IEEE; 2000. p. 904

[7] Dolbilov GV. Two beam proton accelerator for neutron generators and electronuclear industry. In: Proceedings of the 2001 Particle Accelerator Conference; 2001; Chicago, USA. IEEE; 2001. pp. 651-653

[8] Goplen B, Ludeking L, Smithe D, Warren G. MAGIC User' Manual. MRC/WDC-R-409; 1997. DOI: http://www.orbitalatk.com/magic/default.aspx

[9] Teryaev VE, Kazakov SY, Hirshfield JL. Multi-beam linear accelerator EVT. In: Proceedings of EAAC 2015, Nucl. Instr. and Meth. in Phys. Res. A 829; Sept. 13–19, 2015; Isola Elba, Italy; 2016. pp. 221-223. https://www.researchgate.net/publication/301225661_Multi-beam_linear_accelerator_EVT

[10] Teryaev V. Influence of Shape of a Charged Bunch on it's Interaction with the Cavity. KEK Report 2008–9; 2009. Available from: https://www.researchgate.net/publication/265849229_INFLUENCE_OF_SHAPE_OF_A_CHARGED_BUNCH_ON_IT%27S_INTERACTION_WITH_THE_CAVITY_The_engineering_approach

[11] Deruyter H, Mishin A, Roumbanis T, Schonberg R, Farrell S, Smith R, Miller R. High power 2 MeV linear accelerator design characteristics. In: Proceedings of EPAC96; 1996; IEEE; 1996. Available from: http://accelconf.web.cern.ch/accelconf/e96/PAPERS/THPG/THP119G.PDF

[12] Wenlong H, Donaldson CR, Zhang L, Ronald K, Phelps ADR, Cross AW. Numerical simulation of a Gyro-BWO with a helically corrugated interaction region, cusp electron gun and depressed collector. In: Prof. Jan Awrejcewicz, editor. Numerical Simulations of Physical and Engineering Processes. ISBN: 978–953–307-620-1 ed. InTech; 2011. pp. 101-131. https://www.intechopen.com/books/numerical-simulations-of-physical-and-engineering-processes/numerical-simulation-of-a-gyro-bwo-with-a-helically-corrugated-interaction-region-cusp-electron-gun